

Synthesis and characterization of a polyaniline-modified SnO₂ nanocomposite

V. S. Reddy Channu · Rudolf Holze

Received: 23 May 2011 / Revised: 23 November 2011 / Accepted: 27 November 2011 / Published online: 11 December 2011
© Springer-Verlag 2011

Abstract Polyaniline-modified tin oxide and tin oxide nanoparticles were synthesized using a solution route technique. The obtained pristine products were characterized with X-ray diffraction, thermogravimetric analysis, scanning electron microscopy, and optical absorption spectroscopy. Thermogravimetric analysis results showed that the polyaniline-modified SnO₂ nanoparticles exhibit higher thermal stability than the SnO₂ nanoparticles. Scanning electron microscopy analysis on the as-synthesized powders showed spherical particle in the range of 50–100 nm.

Keywords Nanocomposite · Solution route technique · Morphology · Cyclic voltammetry

Introduction

Semiconductor nanoparticles have been studied widely from both experimental and theoretical viewpoints because of their potential applications in the optoelectronic industry, as catalysts, and in solar energy conversion [1–3]. Tin oxide is an *n*-type semiconductor with a large band gap and is well-known for its applications in dye-based solar cells [4] and gas sensors [5]. Recently, attention has been focused on its possible application in electrochemical devices [6]. Rising demand for power sources with high power density has motivated an immense interest in electrochemical supercapacitors in recent years with projected applications in electric vehicles, burst power generation, memory back-up

devices, digital communications, and other related devices which require high pulse power. Supercapacitors have high power density, excellent reversibility, and long cycle life as compared to batteries [7].

In recent years, inorganic–organic nanocomposites have turned into a most attractive subject of research because of their specific physical and chemical properties [8]. Semiconductor–polymer nanocomposites are a particularly promising new field of development of advanced materials in science and technology. The properties of these nanocomposites are quite different from those of the component materials because of interfacial interactions between nanostructured semiconductors and polymers. The properties of these materials can easily be tuned for desired applications through the variation of particle size, shape, and distribution of nanoparticles.

Polypyrrole, polyaniline, and polythiophene have been suggested for applications as active electrode materials in primary and secondary batteries and in supercapacitors [9–11]. Among these polymers, polyaniline has attracted attention because of its environmental stability, good electrical conductivity, and easy synthesis [2]. A synergistic effect in polyaniline–inorganic nanocomposites, particularly, in polyaniline–metal oxide composites, has been applied in electrode materials for supercapacitor. SnO₂ has the benefit of its environmentally benign nature and low cost. It is necessary to prepare and investigate composites combining excellent properties of both polyaniline (PANI) and SnO₂ for electrochemical applications.

Several methods were reported in the literature for the synthesis of PANI–inorganic composite powders and thin films, for example, ex situ intercalation process, drop cast method and in situ self-assembly, and hydrothermal and coprecipitation methods [1, 12–15]. However, to synthesize bulk amounts of fine particles of organic–inorganic powders

V. S. R. Channu (✉) · R. Holze
Institut für Chemie, AG Elektrochemie, Technische Universität
Chemnitz,
09107 Chemnitz, Germany
e-mail: chinare02@gmail.com

requires low temperature and short duration of synthesis. The solution co-precipitation method is suitable to synthesize nanosize PANI–SnO₂ particles [1]. The present work reports on the synthesis of PANI–SnO₂ nanoparticles by a co-precipitation method using citric acid as a carrier.

Experimental

Synthesis of PANI nanoparticles

Aniline was distilled under vacuum; 0.1 M aniline and 1 g citric acid were dissolved in 250 mL of 0.1 M hydrochloric acid and kept below 4 °C for 30 min, and 0.125 M ammonium persulfate (APS) was dissolved in 50 mL of aqueous 0.1 M hydrochloric acid and added to the above solution. The mixed solution was stirred for 2 h, and subsequently, the solution was kept unstirred for further 22 h. The green precipitate was filtrated and washed with a large amount of water, 0.1 M hydrochloric acid, and acetone. The obtained product was dried at 50 °C for 12 h.

Synthesis of SnO₂ nanoparticles

Citric acid (0.1 M) and 0.1 M of tin chloride (SnCl₂·2H₂O) were dissolved in 250 mL of distilled water under mixing with a magnetic stirrer for 4 h. Hydrogen peroxide (H₂O₂) was added to the above solution to oxidize tin ions into tin oxide, and the solution turns into a white-colored suspension of SnO₂. The suspension was aged at 90 °C for 48 h. The white precipitate was filtrated and washed with a large amount of water and C₂H₅OH. It was dried at 100 °C for 8 h and then calcinated at 300 °C for 4 h.

Synthesis of polyaniline-modified SnO₂ nanoparticles

The white-colored suspension of SnO₂ was prepared using the solution route technique described above. It was mixed with 0.1 M aniline and kept below 4 °C in an ice bath. After 30 min, 0.125 M of APS solution was added to the mixture, and the ice bath was removed after a green-colored solution was obtained. The reactant mixture was stirred for 22 h and subsequently aged at 90 °C for 48 h. The green precipitate was filtrated and washed with large amounts of water and acetone. It was dried at 100 °C for 8 h and then calcinated at 250 °C for 4 h. A color change from green to brown was observed after calcination.

Characterization techniques

Crystallographic information of the samples was obtained using an X-ray powder diffractometer STADI P (STOE) with Ge(111) monochromatized Cu-K α radiation ($\lambda =$

1.54187 Å). Diffraction data were collected over the 2 θ range of 20° to 80°. Fourier transform infrared (FTIR) absorption spectra of the nanoparticles were measured using a Bruker IR spectrometer of 4 cm⁻¹ resolution in the 600–4,000-cm⁻¹ range. The morphologies of the resulting products were characterized using a scanning electron microscope (NanoNova SEM of FEI). For thermogravimetric analysis (TGA) measurements, an instrument TGA 7 (Perkin-Elmer) operating in dynamic mode (heating rate=10 °C/min under helium gas) was employed. Optical absorption spectra of equal amounts of SnO₂ and polyaniline-modified SnO₂ nanoparticles dispersed in ethanol were recorded at room temperature in the wavelength region 200–800 nm using a Shimadzu UV–Vis–NIR (Model UV-3100) spectrophotometer. Electrochemical properties of SnO₂ nanoparticles were analyzed by using a three-electrode cell with a platinum counter electrode and a silver wire in a solution saturated with KCl as the reference electrode. The working electrode, prepared by mixing 80 wt.% of active material, 15 wt.% of acetylene black, and 5 wt.% of polyvinylidene fluoride, was coated onto a glassy carbon electrode with a diameter of 5 mm. An aqueous 2.0-mol/L solution of H₂SO₄ was used as the electrolyte. Cyclic voltammetric (CV) measurements were carried out between the potential limits of –0.5 and 1.0 V against Ag/AgCl using a custom-built potentiostat. CV curves were recorded at dE / dt=10 mV s⁻¹.

Results and discussion

Data on phase purity and crystallographic information on the SnO₂ and polyaniline-modified SnO₂ nanoparticles were obtained using powder X-ray diffraction; XRD patterns of nanoparticles are shown in Fig. 1. All diffraction patterns of

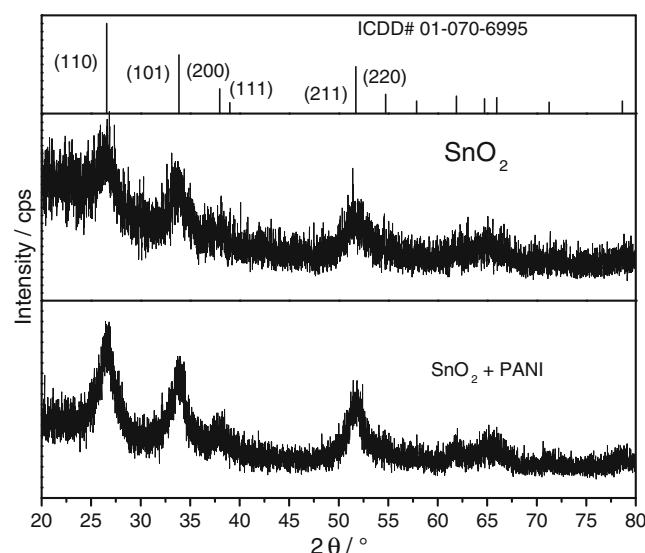


Fig. 1 XRD patterns of SnO₂ and PANI/SnO₂ composite

SnO₂ and polyaniline-modified SnO₂ nanoparticles show characteristic peaks of the tetragonal rutile phase. The XRD patterns are in good agreement with the standard data of the tetragonal rutile phase with $a=4.741 \text{ \AA}$ and $c=3.182 \text{ \AA}$ in close agreement with the standard data file (ICDD # 01-070-6995). No impurity phases were observed. The observed broadening of diffraction peaks in polyaniline-modified SnO₂ indicates incorporation of polyaniline in tin oxide [5].

FTIR spectra of PANI and polyaniline-modified SnO₂ nanocomposite are shown in Fig. 2. PANI exhibits peaks at wavenumbers 1,582, 1,492, 1,302, 1,142, and 805 cm⁻¹ [2]. The peaks at 1,582 and 1,492 cm⁻¹ correspond to C=N- and C=C-stretching modes of the benzenoid rings. The peaks at 1,302 and 1,142 cm⁻¹ are attribute to the C–N-stretching mode of benzenoid rings. The peak at 805 cm⁻¹ is assigned to C–H out-of-plane bending vibrations. All characteristic peaks of PANI can be observed in the FTIR spectrum of polyaniline-modified SnO₂ nanocomposite. However, some peaks of modified PANI have shifted slightly due to interaction with tin oxide.

TGA curves of PANI, SnO₂, and polyaniline-modified SnO₂ precursor are shown in Fig. 3. The weight losses happened in two steps. The first weight loss was 0.69 mg in the temperature range 30–97 °C; this weight loss could be attributed to evaporation of water from the PANI. The second weight loss is 0.62 mg in the temperature range 97–250 °C; it is attributed to decomposition of citric acid. The respective first weight loss was 0.79 mg in SnO₂ in the temperature range 30–195 °C and 0.546 mg in polyaniline-modified SnO₂ in the temperature range 30–122 °C. This first weight loss corresponds to evaporation of water from the metal oxides. The second weight loss was 2.03 mg in

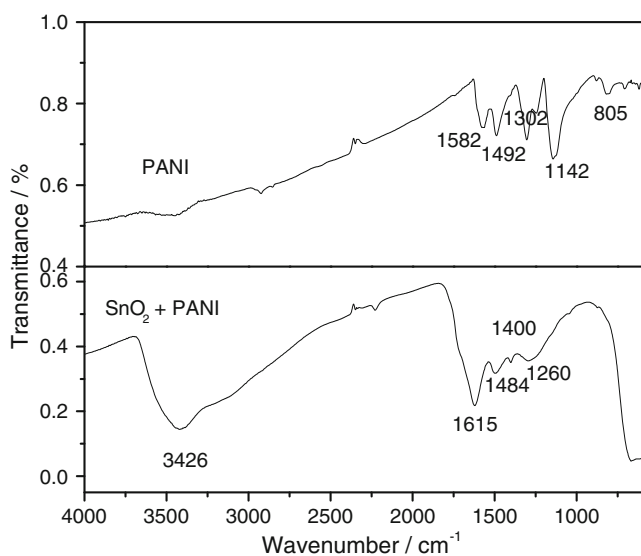


Fig. 2 FTIR spectra of PANI and PANI/SnO₂ composite

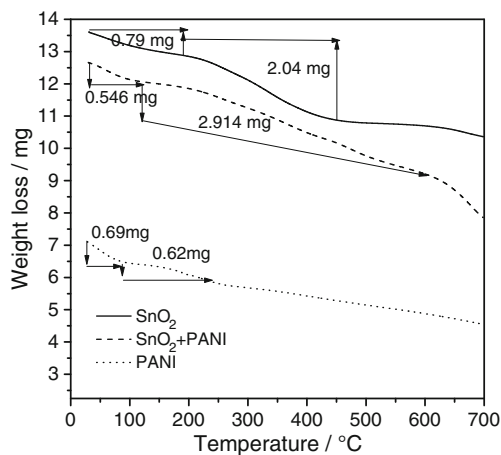


Fig. 3 TG curves of PANI, SnO₂, and PANI/SnO₂ composite

SnO₂ in the temperature range 195–455 °C and 2.914 mg in polyaniline-modified SnO₂ in the temperature range 122–595 °C. This second weight loss can be attributed to decomposition of citric acid in SnO₂ and in polyaniline-modified SnO₂ to decomposition of citric acid and polyaniline. PANI decomposes between 97 and 250 °C, but the SnO₂+ PANI composite decomposes slowly from 120 to 600 °C. This result implies that PANI interacted strongly with the surface SnO₂, enhancing the thermal stability of polyaniline.

Figure 4 shows the UV–Vis absorption spectra of the SnO₂ and polyaniline-modified SnO₂ nanocomposite and PANI. The UV–Vis spectra show absorption peaks at 265 nm for SnO₂ and 270 nm for PANI-modified SnO₂ and 350 nm for PANI. The absorption peak shift from 265 to 270 nm indicates the presence of polyaniline in the composite and a possible increase in π -conjugation of the polymer chains when they are interacted strongly with the

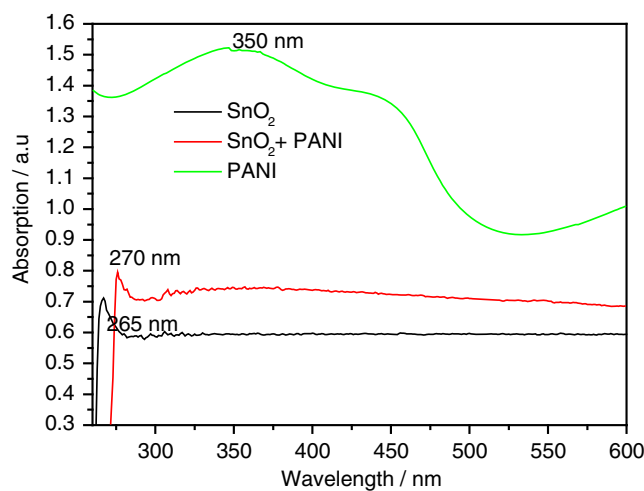


Fig. 4 UV–vis spectra of PANI, SnO₂, and PANI/SnO₂ composite

surface SnO₂. The optical band gap value E_g can be determined from the optical absorption spectra using Tauc's relation [16]:

$$\alpha = A/h \cdot \nu (h \cdot \nu - E_g)^n$$

where α is the absorption coefficient, $h \cdot \nu$ is the photon energy, and A is a constant. For a direct transition, band gap semiconductor E_g can be obtained from the relation

$$\alpha \cdot h \cdot \nu = A(h \cdot \nu - E_g)^{1/2}$$

To calculate direct band gap E_g , one can plot $(\alpha \cdot h \cdot \nu)^2$ vs. $h \cdot \nu$ and extrapolate the linear portion of it to $\alpha = 0$ value yielding the corresponding band gap energy. Plots of $(\alpha \cdot h \cdot \nu)^2$ vs. $h \cdot \nu$ for SnO₂ and PANI-modified SnO₂ are shown in Fig. 5. The calculated band gap energy value for SnO₂ is 4.0 eV and for PANI-modified SnO₂ is 4.2 eV.

For indirect transitions, which require photon assistance, the absorption coefficient has the following dependency on the photon energy

$$\alpha \cdot h \cdot \nu = A[h \cdot \nu - E_g + E_p]^2 + B[h \cdot \nu - E_g - E_p]^2$$

where E_p is the energy of the photon associated with the transition, and A and B are constants depending on the band structure. The band gap energies for indirect transitions were obtained from the plots of $(\alpha \cdot h \cdot \nu)^{1/2}$ vs. photon energy ($h \cdot \nu$) as shown in Fig. 6. The obtained value for SnO₂ is 3.75 eV and for PANI-modified SnO₂ is 4.0 eV.

The position of the absorption edge values was calculated by extrapolating the linear portions of the α vs. $h \cdot \nu$ plot as shown in Fig. 7 to zero absorption value. The calculated absorption edge value for SnO₂ is 3.8 eV and for PANI-modified SnO₂ 4.3 eV. The absorption edge, direct band gap, and indirect band gap energies are higher for PANI-modified SnO₂ than for plain SnO₂. The widening of band gaps occurs with the modification of polyaniline in SnO₂

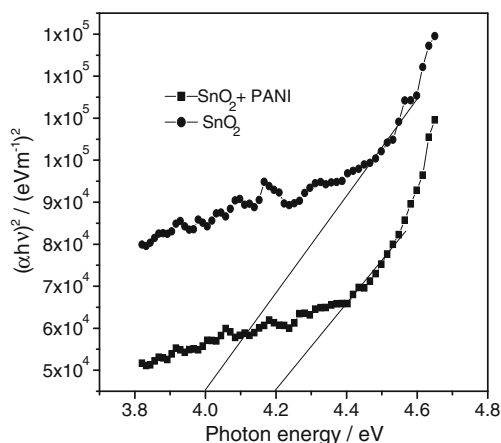


Fig. 5 Plot of $(\alpha h \nu)^2$ vs. $h \nu$ for SnO₂ and PANI/SnO₂ composite

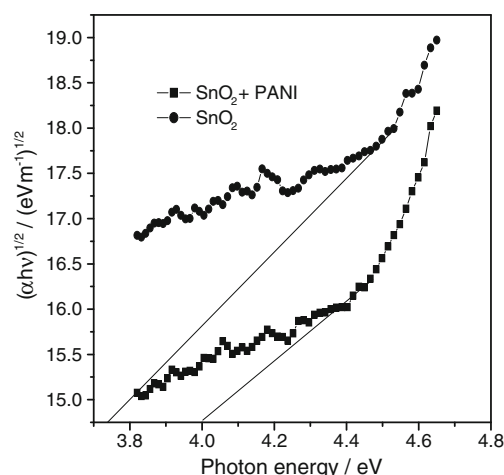


Fig. 6 Plot of $(\alpha h \nu)^{1/2}$ vs. $h \nu$ for SnO₂ and PANI/SnO₂ composite

matrix [1]. Compared to the bulk energy gap (3.6 eV), the higher band gap energy is due to quantum confinement effects of SnO₂ nanoparticles.

SEM images of PANI and PANI-modified SnO₂ nanocomposite are shown in Fig. 8. Polyaniline particles (Fig. 8a) are of spherical shape with diameter in the range from 50 to 100 nm. In Fig. 8b, a doll-like microporous structure of PANI/SnO₂ is observed. According to the SEM images, it appears to be very likely that the nanostructured SnO₂ particles are embedded within PANI chains. This implies that the composite is highly microporous and thus capable of increasing the liquid–solid interfacial area providing more locations for the insertion and extraction of ions, ensuring a higher heterogeneous reaction rate.

The capacitance behavior of SnO₂ and PANI-modified SnO₂ nanoparticles as electrode materials has been studied using 2 M H₂SO₄ electrolyte solution within a potential window of –0.5 to 1.0 V vs. Ag/AgCl by standard cyclic voltammetry. Cyclic voltammograms of SnO₂ nanoparticles

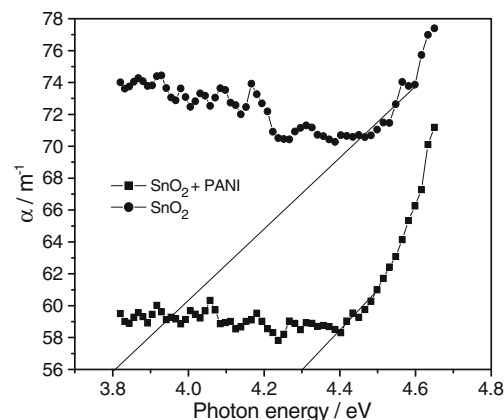


Fig. 7 Plot of α vs. $h \nu$ for SnO₂ and PANI/SnO₂ composite

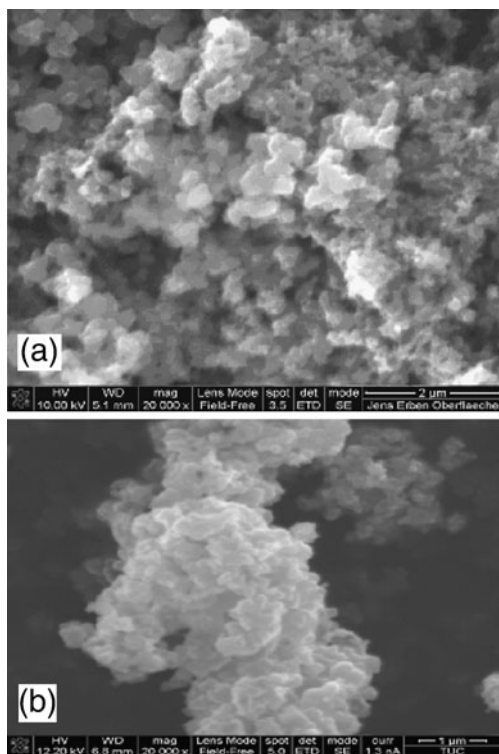


Fig. 8 SEM images of a PANI and b PANI/SnO₂ composite

and PANI-modified SnO₂ nanoparticles are shown in Fig. 9. The CV curves are more or less rectangular in shape within the measured potential window, indicating good charge propagation within the electrode. Less intense anodic and cathodic peaks were observed in CVs of SnO₂ nanoparticles.

The CV of the PANI-modified SnO₂ nanocomposite (Fig. 9b) presents a large pseudocapacitive background current, but it also reveals visible current peaks (P1/P2, P3/P4). The ideal capacitor performance requires that redox processes occur continuously (causing pseudocapacitive behavior). Negative to 0.20 V PANI is in its entirely neutral state, designated as leucomeraldine (LE). At 0.20 V, LE undergoes partial oxidation resulting in the emeraldine (EM) state. If the potential becomes more positive, EM undergoes further oxidation yielding pernigraniline (PE). The oxidation and reduction processes are accompanied by doping and dedoping of counter anions. Since these processes are reversible, charge storage in PANI provides a pseudocapacitance performance [8]. The shape of the curves (Fig. 9b) reveals that the capacitance feature of the PANI-modified SnO₂ nanocomposite electrode is mainly related to the redox mechanism, and in Fig. 9b, two processes of the PANI redox transitions are clearly observed. The anodic and cathodic peaks (P1/P2) correspond to the LE/EM transition. Similarly, the anodic and cathodic peaks are attributed to the EM/PE transition. The occurrence of current peaks (albeit weak

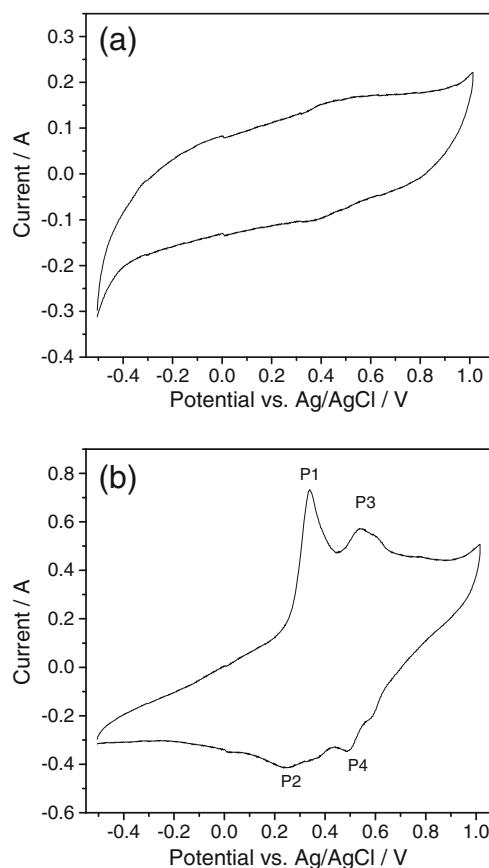


Fig. 9 CV curves of a pure SnO₂ electrode and b PANI/SnO₂ composite electrode at a scan rate of 10 mV/s in 2 M H₂SO₄ aqueous electrolyte; mass of each electrode is 5 mg

ones) is due to the polydispersity of PANI. In case of a complete absence of a most likely chain length (a maximum in a distribution function), chain segments showing conjugation ranging from very short to very long ones would be present resulting in a correspondingly broad distribution of redox peaks actually merged into a capacitive-like current. Apparently, PANI as prepared here does not show this extreme distribution, instead a chain length correlated with the peak positions dominates resulting in the observed behavior.

Conclusions

PANI-modified SnO₂ and SnO₂ nanoparticles were successfully synthesized by a solution route technique using citric acid as a carrier. Scanning electron microscopy analysis of the as-synthesized powders showed spherical particles with sizes in the range of 50–100 nm. Electrochemical results indicate that the PANI-modified SnO₂ composite had a higher background current with apparent cathodic and anodic peaks.

Acknowledgments One of the authors (VSRC) thanks the Alexander von Humboldt-Foundation for a fellowship. The authors gratefully acknowledge the valuable contributions by Maik Schlesinger and Michael Mehring's group in the structural analysis using XRD.

References

1. Dutta K, De SK (2007) *Mater Lett* 61:4967
2. Haili P, Changting H, Jinhua C, Bo L, Yafei K, Xiaohua Z (2010) *J Solid State Electrochem* 14:169
3. Barsan N, Weimar U (2003) *J Phys Condens Matter* 15:R813
4. Srivastava DN, Chappel S, Palchik O, Zaban A, Gedanken A (2002) *Langmuir* 18:4160
5. Deshpande NG, Gudage YG, Ramphal Sharma, Vyas JC, Kim JB, Lee YP (2009) *Sens Actuators B* 138:76.
6. Zhu J, Lu Z, Aruna ST, Aurbach D, Gedanken A (2000) *Chem Mater* 12:2557
7. Conway BE (1999) *Electrochemical supercapacitors: scientific fundamentals and technological applications*. Kluwer Academic/Plenum, New York
8. Zhong-Ai H, Yu-Long X, Yao-Xian W, Li-Ping M, Yu-Ying Y, Zi-Yu Z (2009) *Mater Chem Phys* 114:990
9. Liang HC, Chen F, Li RG, Wang L, Deng ZH (2004) *Electrochim Acta* 49:3463
10. Aurian-Blajeni B, Beebe X, Rauh RD, Rose TL (1989) *Electrochim Acta* 34:795
11. Kim YT, Tadai K, Mitani T (2005) *J Mater Chem* 15:4914.
12. Ma X, Wang M, Li G, Chen H, Bai R (2006) *Mater Chem Phys* 98:241
13. Ram MK, Yavuz O, Lahsangah V, Aldissi M (2005) *Sens Actuators B* 106:750
14. Huiling T, Yadong J, Guangzhong X, Junsheng Y (2010) *J Mater Sci Technol* 26:605.
15. Lina G, Yingqiang Z, Xueliang H, Shurong W, Shoumin Z, Shihua W (2007) *Sens Actuators B* 120:568
16. Thutupalli GM, Tomlin SG (1976) *J Phys D: Appl Phys* 9:1639